JAERI-Tech
96-016

OPTIMIZING VOLTAGE WAVE FORMS OF POLOIDAL FIELD COILS AT THE PLASMA BREAKDOWN

March 1996

Ikuo SENDA[*1], Teruaki SHOJI, Toru NISHINO[*2], Hirobumi FUJIEDA[*3]
and Toshihide TSUNEMATSU

日本原子力研究所
Japan Atomic Energy Research Institute

本レポートは，日本原子力研究所が不定期に公刊している研究報告書です。

入手の問合わせは，日本原子力研究所技術情報部情報資料課（〒319-11 茨城県那珂郡東海村）あて，お申し越しください。なお，このほかに財団法人原子力弘済会資料センター（〒319-11 茨城県那珂郡東海村日本原子力研究所内）で複写による実費頒布をおこなっております。

This report is issued irregularly.

Inquiries about availability of the reports should be addressed to Information Division, Department of Technical Information, Japan Atomic Energy Research Institute, Tokai-mura, Naka-gun, Ibaraki-ken 319-11, Japan.

編集兼発行　日本原子力研究所

印　　刷　㈱原子力資料サービス

Optimizing Voltage Wave Forms of Poloidal Field Coils at the Plasma Breakdown

Ikuo SENDA*1, Teruaki SHOJI, Toru NISHINO*2
Hirobumi FUJIEDA*3 and Toshihide TSUNEMATSU

Department of ITER Project
Naka Fusion Research Establishment
Japan Atomic Energy Research Institute
Naka-machi, Naka-gun, Ibaraki-ken

(Received March 4, 1996)

BreakDown Optimization and Simulation (BDOS) code is developed, in which the voltage wave forms of the poloidal field coils are optimized during plasma breakdown so that the poloidal error fields in the breakdown region are minimized and the one-turn voltage at the center of the region becomes the assigned value. The effect of eddy currents induced in the in-vessel components is taken into account by eigen-mode analysis using the finite element method.

As an example, the breakdown optimization is studied using the reference plasma in the interim design of International Thermonuclear Experimental Reactor engineering design activity. It is shown that optimization of the voltage wave form of poloidal field coils enables minimization of error fields as low as 2mT in the breakdown region, which is a circle of 1m radius, when one-turn voltage at the center is about 17V. The capability of cancelling error fields by optimizing coils' voltage wave forms is investigated in the cases with different one-turn voltages at the center of the breakdown region. We find that the reduction of one-turn voltage as low as 10V makes it possible to recover error field pattern of the initial magnetization, where we obtain a low error field region of less than 2mT in a circular of 1.5m radius. Another finding is that the duration of keeping small error field in the breakdown region increases rapidly as the one-turn voltage decreases.

Keywords: Breakdown, Error Field, Eddy Current, ITER, EDA

---

*1 On loan from Toshiba Corporation
*2 Kanazawa Computer Service
*3 Atomic Energy General Service Corporation

プラズマブレークダウン時のポロイダルコイル電圧波形の最適化

日本原子力研究所那珂研究所ＩＴＥＲ開発室
仙田　郁夫*1・荘司　昭朗・西野　　徹*2
藤枝　浩文*3・常松　俊秀

（1996年３月４日受理）

プラズマブレークダウン（点火）時にプラズマ点火領域に生ずる誤差磁場を低減するようにポロイダル磁場コイルの制御電圧波形を最適化し，その時の磁場配位の時間発展をシミュレーションするためのコード，BDOS(BreakDown Optimization and Simulaton)-code,を開発した。このコードは，プラズマ点火領域の中の指定された何点かに於けるポロイダル磁場を最小にし，その領域中心での一周誘導電圧を指定された値にするように，ポロイダル磁場コイルの電圧を最適化する。炉内構造物は有限要素法によりモデル化し，そこに誘起される渦電流は薄板近似を用いた回路方程式の固有モード解析を行った結果を使って求める。

ITER EDA の中間報告書にある標準設計の場合について，プラズマ点火時の誤差磁場低減の解析を行った。コイル電圧を最適化することにより，一周誘導電圧17V程度のとき，誤差磁場２mT以下の領域を半径１mの円形状領域にわたってを作ることができることを示した。また，誤差磁場の配位が一周電圧にどのように依存するか検討を行った。その結果，一周電圧を10V程度に低減するならば，コイル電圧波形を最適化することにより，初期励磁の時とほぼ同程度の低磁場領域を得ることを示した。このとき，半径1.5mより大きな円形領域で２mT以下の低誤差磁場領域が得られる。また，低誤差磁場の領域を維持できる時間の長さは，一周電圧を減少させると急速に長くなることを示した。

那珂研究所：〒311-01　茨城県那珂郡那珂町向山801-1
*1　㈱ 東芝より出向中
*2　㈱ カナザワコンピュータサービス
*3　㈱ 原子力資料サービス

Contents

目　　次

1, Introduction

To initiate a discharge of the Tokamak reactor, magnetic flux must be supplied to the breakdown region externally by poloidal field (PF) coils. Depending on the time change rate of the supplied flux, one-turn voltage is given to the gas in Tokamak. When the ionized electrons run sufficiently long distance in the toroidal direction, the plasma toroidal current is created and then the discharge is initiated, namely Townsend avalanche [1]. However, in the presence of large poloidal error fields, the trajectories of the plasma particles go out of the breakdown region and the plasma breakdown may fail. Therefore, in designing Tokamak reactor, much attention is payed to reduce the error field during the break down of the plasma so that the plasma toroidal current is maintained.

The structure of the Tokamak reactor is determined not only by the advantage on plasma breakdown, but as a compromise with demands arising from the other aspects of the reactor design. Therefore, the reactor design is not necessarily optimized with respect to the plasma breakdown. In the case that large error field is expected at plasma breakdown, the optimization of the control voltages of PF coils and the auxiliary heating control must be performed within the design limitation in order to maintain better conditions of the plasma breakdown[2].

In the engineering design of International Thermonuclear Experimental Reactor (ITER), the one-turn resistance of in-vessel component is designed to have a small value in order to obtain stability of the plasma[3]. On the other hand, small one-turn resistance of in-vessel components poses a problem to the plasma breakdown as large error fields are created during rapid change of poloidal flux at the plasma initiation. In this case, optimization of PF voltage wave form is essential so that the cancellation of error fields created by PF coils and eddy currents occurs. Since such optimization depends on the details of the passive structures, the modeling of the structures should be carried out carefully.

For the purpose of optimizing PF coil voltage wave form during the plasma breakdown, BreakDown Optimization and Simulation (BDOS) code was developed. BDOS code optimizes PF coil voltage wave form, given the breakdown position, plasma one-turn voltage, the limitation of PF coil voltages and resisters inserted to PF coils. BDOS code has several important features. One of them is that BDOS code solves eddy currents induced on in-vessel components by using the results of EDDYCAL code, which models the in-vessel components by finite element method and analyzes the eigen modes of the induced currents[4]. Therefore, 3-dimensional structure of the current path is taken into account and the precise modelings of in-vessel components are possible.

The dependence of the breakdown region on the one-turn voltage was studied using BDOS code. The case we treated in this report is the reference design of ITER EDA interim report, which has a layer CS coil and 7 outer PF coils. The toroidal one-turn resistance of in-vessel structure (vacuum vessel, back plate and blanket shield modules) is about 5 micro ohm in the present analysis. The reference one-turn voltage of plasma at the breakdown is 16V and the requirement of the plasma breakdown is that the error field in the breakdown region should be at least less than 2mT. If one applies 16V of one-turn voltage by flux supply without optimizing PF coil voltages, the error field in the breakdown region becomes more than 10mT and the plasma initiation is almost impossible. As a result of analysis, we found that there are wave forms of PF coils' voltages which minimize error fields as low as 2mT in the breakdown region.

The reduction of one-turn voltage required during plasma breakdown has been demonstrated experimentally with the help of additional heating. For example JFT-2M showed that one-turn voltage can be reduced as low as 1/10 at the plasma breakdown with ECH assist compared with the breakdown without ECH[5]. Since induced eddy currents become small as one-turn voltage becomes low, it also has an advantage in reducing error field and obtaining larger breakdown region. In the following, we also report the dependence of the breakdown region, where error field is less than 2mT, on the one-turn voltage during breakdown and show that reducing one-turn voltage by 50% makes it easier to obtain large breakdown region.

This report is organized as follows. In section 2, the mathematical formulation of BDOS code is presented. In section 3, the method of optimizing coil voltages is explained. Section 4 describes results of analysis using BDOS code in the example of the reference in interim ITER EDA design. Section 5 is a summary.

2, Mathematical formulation

BreakDown Optimization and Simulation (BDOS) code solves coupled equations of coil and eddy currents' circuit equations. Since the coupling between poloidal field (PF) coils and eddy currents are constants, their time evolutions are solved exactly once the voltages of PF coils are given. The basic inputs and assumptions of BDOS code are the follows.

1) The eddy currents induced on the in-vessel components are solved by finite element method.
2) The initial condition of current flowing in PF coils is computed with the other codes[6] and given to BDOS code.
3) Time change of PF coils' resistances inserted during the breakdown is given.
4) The time changes of PF coils' voltages are assumed to be linear in time between time slices, where applied voltages are optimized.

The circuit equations of PF coils and eddy currents are given by,

$$\begin{aligned} &\sum_{k}^{coil} M_{j,k}\dot{I}_k + \sum_{\alpha}^{eddy} G_{j,\alpha}\dot{X}_\alpha + \eta_j I_j = V_j \\ &\sum_{k}^{coil} G_{k,\alpha}\dot{I}_k + D_\alpha \dot{X}_\alpha + X_\alpha = 0 \end{aligned} \quad , \tag{1}$$

where dots on variables mean the time derivatives, I_j is the current of j-th PF coil and X_α is α-th eigen mode of eddy currents. The symbol $M_{j,k}$ stands for magnetic couplings between PF coils and $G_{j,\alpha}$ stands for coupling between j-th PF coil and α -th eddy mode. The resistance of j-th PF coil is given by η_j, PF coil voltage V_j and the eigen value of α-th eigen mode is indicated by D_α. These equations are summarized by a single equation by,

$$M \cdot \dot{Y} + R \cdot Y = B \quad , \tag{2}$$

where matrices and vectors are defined by,

$$M=\begin{pmatrix} \ddots & & & \vdots & \\ & M_{i,j} & \cdots & G_{i,\alpha} & \cdots \\ & & \ddots & \vdots & \\ & \vdots & \ddots & & 0 \\ \cdots & G_{\alpha,j} & \cdots & D_{\alpha} & \\ & \vdots & 0 & & \ddots \end{pmatrix},$$

$$R_{Diagonal}=\begin{pmatrix} \cdots & \eta_i & \cdots & \cdots & 1 & \cdots \end{pmatrix},$$

$$Y={}^{T}\begin{pmatrix} \cdots & I_i & \cdots & \cdots & X_{\alpha} & \cdots \end{pmatrix},$$

$$B={}^{T}\begin{pmatrix} \cdots & V_i & \cdots & \cdots & 0 & \cdots \end{pmatrix}.$$

In the followings, we assume that the number of PF coils is N_C and the number of eigen modes of eddy currents is N_E.

To solve eq. (2), it is convenient to separate coils with zero resistance and non-zero resistance. The matrix U_r is defined so that it rearranges between coils with zero and non-zero resistances,

$$\begin{aligned} &U_r^{-1}\cdot R\cdot U_r=R_r \\ &(R_r)_{Diag}=(0,\cdots 0,\eta_1,\cdots,\eta_{N2},1\cdots 1) \end{aligned} \tag{3}$$

In eq.(3), the number of PF coils is divided into N_1 coils with zero resistances and N_2 coils with non-zero resistances. Equation (2) is rewritten as,

$$\begin{aligned} &M_r\cdot\dot{Y}_r+R_r\cdot Y_r=B_r \\ &M_r\equiv U_r^{-1}\cdot M\cdot U_r,\quad Y_r\equiv U_r^{-1}Y,\quad B_r\equiv U_r^{-1}B \end{aligned} \tag{4}$$

Equation (4) is transformed further by introducing matrix U_S. Let us redefine quantities in eq.(4) by,

$$\begin{aligned} &(U_S)_{Diag}=(1,\cdots 1,1/\sqrt{\eta_1},\cdots,1/\sqrt{\eta_{N2}},1,\cdots 1) \\ &U_S\cdot R_r\cdot U_S\equiv R_S,\quad (R_S)_{Diag}=(0,\cdots 0,1,\cdots 1,1,\cdots 1) \\ &U_S\cdot M_r\cdot U_S\equiv M_S,\quad U_S^{-1}\cdot Y_r\equiv Y_S \end{aligned} \tag{5}$$

where diagonal part of R_S has N_1 zeros and (N_2+N_E) 1s. Equation (5) transforms eq.(4) and quantities in it as follows,

$$\dot{Y}_S + M_S^{-1} \cdot R_S \cdot Y_S = M_S^{-1} \cdot U_S \cdot B_r$$
$$Y_S \equiv \begin{pmatrix} Y^{(1)} \\ Y^{(2)} \end{pmatrix}, \quad M_S^{-1} \cdot R_S \equiv \begin{pmatrix} 0 & \tilde{M}^{(1)} \\ 0 & \tilde{M}^{(2)} \end{pmatrix}, \quad M_S^{-1} \cdot U_S \cdot U_r \equiv \begin{pmatrix} \tilde{B}^{(1)} \\ \tilde{B}^{(2)} \end{pmatrix}, \tag{6}$$

where $Y^{(1)}$ is a vector including PF coils with zero resistance (N_1 rows) and $Y^{(2)}$ is a vector of PF coils with non-zero resistance and eddy currents ($N_2 + N_E$ rows). Then, the differential equation is divided into two parts,

$$\begin{cases} \dot{Y}^{(1)} + \tilde{M}^{(1)} \cdot Y^{(2)} = \tilde{B}^{(1)} \cdot B \\ \dot{Y}^{(2)} + \tilde{M}^{(2)} \cdot Y^{(2)} = \tilde{B}^{(2)} \cdot B \end{cases} \tag{7}$$

Differential equations in eq.(7) are solved using results of eigen mode analysis of matrix $\tilde{M}^{(2)}$. Since $\tilde{M}^{(2)}$ is a real symmetric $(N_2 + N_E) \times (N_2 + N_E)$ matrix, it is diagonalized by a similarity transformation by a matrix U_2,

$${}^T U_2 \cdot \tilde{M}^{(2)} \cdot U_2 = \tilde{M}^{(2)}_{Diag}, \quad \left(\tilde{M}^{(2)}_{Diag}\right)_{i,i} = A_i^{(2)} \tag{8}$$

Then eq.(7) is rewritten as,

$$\tilde{Y}^{(2)} \equiv {}^T U_2 \cdot Y^{(2)}$$
$$\dot{Y}^{(1)} + \tilde{M}^{(1)} \cdot U_2 \cdot \tilde{Y}^{(2)} = \tilde{B}^{(1)} \cdot B \tag{9}$$
$$\dot{\tilde{Y}}^{(2)} + \tilde{M}^{(2)}_{Diag} \cdot \tilde{Y}^{(2)} = {}^T U_2 \cdot \tilde{B}^{(2)} \cdot B$$

After transformations in eqs. (8) and (9), Vector Y in eq.(2) is given in terms of $Y^{(1)}$ and $\tilde{Y}^{(2)}$ by,

$$Y = U_r \cdot U_S \cdot \begin{pmatrix} Y^{(1)} \\ U_2 \cdot \tilde{Y}^{(2)} \end{pmatrix} \tag{10}$$

The B vector in eq.(2), which contains control voltages, is redefined by introducing a matrix K,

$$B = K \cdot V, \quad V = \begin{pmatrix} V_1 \\ \vdots \\ V_{N_C} \end{pmatrix}, \quad K = \begin{pmatrix} 1 & & 0 \\ & \ddots & \\ 0 & & 1 \\ \hline & \vdots & \\ \cdots & 0 & \cdots \\ & \vdots & \end{pmatrix} \tag{11}$$

As we have mentioned before, the time evolutions of PF coils' voltages between two

time slices t_1 and t_2 are assumed to be linear. The linear evolution of coil voltages from time t_1 to t_2 is give by,

$$V_i(t) = V_i(t_1) + \frac{V_i(t_2) - V_i(t_1)}{\delta t}\left(t - t_1 \right), \qquad i = 1 \sim N_C\ , \quad N_C = N_1 + N_2 \quad . \tag{12}$$

Then i-th component of the differential equation with respect to $\tilde{Y}^{(2)}$ in eq.(9) has a simple form, $\dot{Y}_i + a_i Y_i = c_i + b_i t$, which has an analytic solution. Inserting the solution of $\tilde{Y}^{(2)}$ into the first differential equation in eq.(9), the solution to $Y^{(1)}$ is obtained.

Solutions are summarized in a simple form,

$$\begin{aligned} Y_i^{(1)}(t_2) &= S_i^{(1)} + \sum_j T_{i,j}^{(1)} \cdot V_j(t_2) \\ \tilde{Y}_i^{(2)}(t_2) &= \tilde{S}_i^{(2)} + \sum_j \tilde{T}_{i,j}^{(2)} \cdot V_j(t_2) \end{aligned} \quad , \tag{13}$$

where S and T are functions of currents and voltages at t_1. Defining a matrix UF,

$$UF = {}^{T}U_2 \cdot \tilde{B}^{(2)} \cdot K \quad , \tag{14}$$

$S_i^{(1)}$ and $T_{i,j}^{(1)}$ in eq.(13) are given by,

$$S_i^{(1)} = Y_i^{(1)}(t_1) - \left(\tilde{M}^{(1)} \cdot U_2 \cdot I^A \right)_i + \frac{\delta t}{2}\left(\tilde{B}^{(1)} \cdot K \cdot V(t_1) \right)_i \quad ,$$

$$T_{i,j}^{(1)} = \frac{\delta t}{2}\left(\tilde{B}^{(1)} \cdot K \right)_{i,j} - \left(\tilde{M}^{(1)} \cdot U_2 \cdot I^B \right)_{i,j} \quad ,$$

$$I_i^A = \frac{1}{A_i^{(2)}}\left(1 - e^{-A_i^{(2)} \cdot \delta t} \right) \tilde{Y}_i^{(2)}(t_1) + \left\{ -\frac{1}{\delta t}\left[\frac{\delta t}{A_i^{(2)}}\left(\frac{t_1 + t_2}{2} - \frac{1}{A_i^{(2)}} \right) + \frac{1}{\left(A_i^{(2)} \right)^2}\left(\frac{1}{A_i^{(2)}} - t_1 \right)\left(1 - e^{-A_i^{(2)} \cdot \delta t} \right) \right] \right.$$
$$\left. + \left(1 + \frac{t_1}{\delta t} \right) \frac{1}{A_i^{(2)}}\left[\delta t - \frac{1}{A_i^{(2)}}\left(1 - e^{-A_i^{(2)} \cdot \delta t} \right) \right] \right\} \left(UF \cdot V(t_1) \right)_i \ ,$$

$$I_{i,j}^B = \left\{ \frac{1}{\delta t}\left[\frac{\delta t}{A_i^{(2)}}\left(\frac{t_1 + t_2}{2} - \frac{1}{A_i^{(2)}} \right) + \frac{1}{\left(A_i^{(2)} \right)^2}\left(\frac{1}{A_i^{(2)}} - t_1 \right)\left(1 - e^{-A_i^{(2)} \cdot \delta t} \right) \right] \right.$$
$$\left. - \frac{t_1}{\delta t} \frac{1}{A_i^{(2)}}\left[\delta t - \frac{1}{A_i^{(2)}}\left(1 - e^{-A_i^{(2)} \cdot \delta t} \right) \right] \right\} (UF)_{i,j} \quad , \tag{15}$$

where δt is the time step, $\delta t = t_2 - t_1$. Similarly, $\tilde{S}_i^{(2)}$ and $\tilde{T}_{i,j}^{(2)}$ in eq.(13) are defined by,

$$\tilde{S}_i^{(2)} = \tilde{Y}_i^{(2)}(t_1)e^{-A_i^{(2)}\cdot\delta t} + \left\{-\frac{1}{\delta t}\left[\frac{1}{A_i^{(2)}}\left(t_2-\frac{1}{A_i^{(2)}}\right)+\frac{1}{A_i^{(2)}}\left(\frac{1}{A_i^{(2)}}-t_1\right)e^{-A_i^{(2)}\cdot\delta t}\right]+\left(1+\frac{t_1}{\delta t}\right)\frac{1}{A_i^{(2)}}\left(1-e^{-A_i^{(2)}\cdot\delta t}\right)\right\}\left(UF\cdot V(t_1)\right)_i,$$

$$\tilde{T}_{i,j}^{(2)} = \left\{\frac{1}{\delta t}\left[\frac{1}{A_i^{(2)}}\left(t_2-\frac{1}{A_i^{(2)}}\right)+\frac{1}{A_i^{(2)}}\left(\frac{1}{A_i^{(2)}}-t_1\right)e^{-A_i^{(2)}\cdot\delta t}\right]-\frac{t_1}{\delta t}\frac{1}{A_i^{(2)}}\left(1-e^{-A_i^{(2)}\cdot\delta t}\right)\right\}UF_{i,j} \quad . \tag{16}$$

Thus, using equations in eq.(10) and eq.(13), coil currents and eddy currents at time t_2 are determined as functions of quantities at t_1 and control voltage at t_2.

3, Optimization method of the coil voltages

The applied voltages of PF coils are adjusted so that the error fields at several reference points are cancelled and a time change rate of flux at a center of the breakdown region becomes the assigned value. The positions minimizing error fields and the center position of the breakdown region are assumed to be given in the computation. If the number of positions minimizing error fields is N_{BREF}, the poloidal fields $\left(B_R^{(k)}, B_Z^{(k)}\right), k=1\sim N_{BREF}$ and flux Ψ at the center of the breakdown region are related linearly to the currents,

$$B_R^{(k)} = \sum_i BM_{R,i}^{(k)}\cdot Y_i, \quad B_Z^{(k)} = \sum_i BM_{Z,i}^{(k)}\cdot Y_i \quad , \quad k=1\sim N_{BREF}$$
$$\Psi = \sum_i \tilde{\Psi}_i Y_i \tag{17}$$

Using results obtained in section 2, $\left(B_R^{(k)}, B_Z^{(k)}\right)$ and Ψ at time t_2 are given by quantities at t_1 and voltage at t_2 ,

$$B_R^{(k)}(t_2) = F_R^{(k,0)}(t_1) + \sum_j F_{R,j}^{(k,1)} V_j(t_2)$$
$$B_Z^{(k)}(t_2) = F_Z^{(k,0)}(t_1) + \sum_j F_{Z,j}^{(k,1)} V_j(t_2) \quad , \tag{18}$$
$$\Psi(t_2) = \Psi^{(0)}(t_1) + \sum_j \Psi_j^{(1)} V_j(t_2)$$

where coefficients are given by,

$$\tilde{S}_i^{(2)} = \tilde{Y}_i^{(2)}(t_1)e^{-A_i^{(2)}\cdot\delta t} + \left\{-\frac{1}{\delta t}\left[\frac{1}{A_i^{(2)}}\left(t_2-\frac{1}{A_i^{(2)}}\right)+\frac{1}{A_i^{(2)}}\left(\frac{1}{A_i^{(2)}}-t_1\right)e^{-A_i^{(2)}\cdot\delta t}\right]+\left(1+\frac{t_1}{\delta t}\right)\frac{1}{A_i^{(2)}}\left(1-e^{-A_i^{(2)}\cdot\delta t}\right)\right\}\left(UF\cdot V(t_1)\right)_i,$$

$$\tilde{T}_{i,j}^{(2)} = \left\{\frac{1}{\delta t}\left[\frac{1}{A_i^{(2)}}\left(t_2-\frac{1}{A_i^{(2)}}\right)+\frac{1}{A_i^{(2)}}\left(\frac{1}{A_i^{(2)}}-t_1\right)e^{-A_i^{(2)}\cdot\delta t}\right]-\frac{t_1}{\delta t}\frac{1}{A_i^{(2)}}\left(1-e^{-A_i^{(2)}\cdot\delta t}\right)\right\}UF_{i,j} \quad . \tag{16}$$

Thus, using equations in eq.(10) and eq.(13), coil currents and eddy currents at time t_2 are determined as functions of quantities at t_1 and control voltage at t_2.

3, Optimization method of the coil voltages

The applied voltages of PF coils are adjusted so that the error fields at several reference points are cancelled and a time change rate of flux at a center of the breakdown region becomes the assigned value. The positions minimizing error fields and the center position of the breakdown region are assumed to be given in the computation. If the number of positions minimizing error fields is N_{BREF}, the poloidal fields $\left(B_R^{(k)}, B_Z^{(k)}\right), k=1\sim N_{BREF}$ and flux Ψ at the center of the breakdown region are related linearly to the currents,

$$B_R^{(k)} = \sum_i BM_{R,i}^{(k)}\cdot Y_i, \quad B_Z^{(k)} = \sum_i BM_{Z,i}^{(k)}\cdot Y_i \quad , \quad k=1\sim N_{BREF}$$
$$\Psi = \sum_i \tilde{\Psi}_i Y_i \tag{17}$$

Using results obtained in section 2, $\left(B_R^{(k)}, B_Z^{(k)}\right)$ and Ψ at time t_2 are given by quantities at t_1 and voltage at t_2 ,

$$B_R^{(k)}(t_2) = F_R^{(k,0)}(t_1) + \sum_j F_{R,j}^{(k,1)} V_j(t_2)$$
$$B_Z^{(k)}(t_2) = F_Z^{(k,0)}(t_1) + \sum_j F_{Z,j}^{(k,1)} V_j(t_2) \quad , \tag{18}$$
$$\Psi(t_2) = \Psi^{(0)}(t_1) + \sum_j \Psi_j^{(1)} V_j(t_2)$$

where coefficients are given by,

$$F_R^{(k,0)}(t_1) = \sum_j^{N1} BY_{R,j}^{(k)} S_j^{(1)} + \sum_j^{N2+NE} BY_{R,j}^{(k)} \left(U_2 \cdot \tilde{S}_i^{(2)}\right)_j \quad ,$$

$$F_{R,j}^{(k,1)} = \sum_l^{N1} BY_{R,l}^{(k)} T_{l,j}^{(1)} + \sum_l^{N2+NE} BY_{R,l}^{(k)} \left(U_2 \cdot \tilde{T}^{(2)}\right)_{l,j} \quad ,$$

$$\Psi^{(0)}(t_1) = \sum_j^{N1} FY_j S_j^{(1)} + \sum_j^{N2+NE} FY_j \left(U_2 \cdot \tilde{S}_i^{(2)}\right)_j \quad ,$$

$$\Psi_j^{(1)} = \sum_l^{N1} FY_l T_{l,j}^{(1)} + \sum_l^{N2+NE} FY_l \left(U_2 \cdot \tilde{T}^{(2)}\right)_{l,j} \quad , \tag{19}$$

$$BY_{R,j}^{(k)} = \sum_i BM_{R,i}^{(k)} \left(U_r \cdot U_S\right)_{i,j} \quad ,$$

$$BY_{Z,j}^{(k)} = \sum_i BM_{Z,i}^{(k)} \left(U_r \cdot U_S\right)_{i,j} \quad ,$$

$$FY_j = \sum_i \tilde{\Psi}_i \left(U_r \cdot U_S\right)_{i,j} \quad .$$

Coefficients of B_Z are obtained similarly to those of B_R.

In order to optimize coil voltages, we define positive definite function Q by,

$$\begin{aligned} Q &= \sum_{k=1}^{N_{BREF}} \left[q_R^{(k)} \left(B_R^{(k)}(t_2)\right)^2 + q_Z^{(k)} \left(B_Z^{(k)}(t_2)\right)^2 \right] + q^{\Psi} \left(\dot{\Psi}(t_2) - \dot{\Psi}_{REF}\right)^2 \\ &= Q^{(0)} + Q^{(1)} \cdot V(t_2) + V(t_2) \cdot Q^{(2)} \cdot V(t_2) \end{aligned} \quad , \tag{20}$$

where q's are weights of poloidal error fields and the time derivative of the flux at given positions. The quantity $\dot{\Psi}_{REF}$ is the reference value of the change rate of flux at the center of the breakdown region. As shown in the second line of eq.(20), Q is a quadratic function of voltage at time t_2 and their coefficients are combinations of quantities introduced in eq.(19). BDOS code allows temporal variation of weights q in eq.(20).

Since there are upper and lower limits of coil voltages due to limited power supply capability, optimization of voltages V is performed to minimize the function Q in eq.(20) within the limitation. Unfortunately, the least square method is not suitable to minimize eq.(20) in the presence of the limitation on voltages. We use the most primitive but the most reliable method to find a global minimum, namely computing Q in eq.(20) through the allowed area of voltages and find a minimum. The flow diagram of BDOS code is shown in Fig. 1. Starting with initial conditions, the coefficients in function Q are computed. Next step is to find a vector of control voltage which minimizes Q. The procedure is repeated until the end of computation.

4, The dependence of the capability in cancelling error fields on the applied one-turn voltage

As mentioned in section 1, it is important to investigate the capability of PF coils in cancelling the error field for different one-turn voltages at the breakdown region. This problem was investigated using BDOS code. As an example, we use the reference design of interim report in ITER EDA. The poloidal cross section is shown in Fig. 2. There are 8 PF coils, namely one layer CS coil and 7 outer coils. As explained in section 1, in-vessel components are modeled by finite element method and eigenvalue analysis is done by EDDYCAL code. The model of passive structure used in the analysis is shown in Fig. 3. The components included in Fig. 3 are the vacuum vessel (one-turn resistance = $13.2\mu\Omega$), the back plate ($14.2\mu\Omega$) and the first wall ($20\mu\Omega$). The currents in PF coils at the initial magnetization is computed by INIMAG code, which determines coil currents so that error fields at the breakdown region become small and the flux at the center of the region equals to a given value. The poloidal error fields at the initial magnetization is shown in Fig.4, in which one sees that the area of small error field (<2mT) is larger than a circle of 1.5m radius centered at $(R,Z)=(9.5,0.0)$m.

The position of the center of the breakdown region is

$$(R,Z)_{CENTER\ Break\ down}=(9.5,0.0)\quad,\quad unit=meter\quad .$$

The positions to minimize poloidal error fields are chosen to the center (9.5,0)m and 4 points on the circle of the 1m radius from the center,

$$\begin{aligned} Center &= (9.5,0.0) \\ In &= (8.5,0.0)\,,\quad Up = (9.5,1.0) \\ Out &= (10.5,0.0)\,,\quad Down = (9.5,-1.0) \end{aligned}\quad , \tag{21}$$

where unit is meter. The resisters are inserted in CS, PF2 and PF7 coils so that the flux is supplied to plasma and no active control voltages are applied to these coils. Coils PF3, 4, 5, 6 and 8 are controlled by booster converters with limited capacities,

$$|V_3|<44V/turn,\quad |V_4|<30V/turn,\quad |V_5|<34V/turn,\quad |V_6|<38V/turn,\quad |V_8|<45V/turn.$$

Thus, the optimization of control voltages is performed in these limitations.

A first example, in which the one-turn voltage at the breakdown is about 17V ($\approx 0.28V/m$), is investigated. The resistances of CS, PF2 and PF7 are,

$$\begin{aligned} CS &: \ 1.16\times10^{-7}\,\Omega/turn^2 \\ PF2 &: \ 2.00\times10^{-6}\,\Omega/turn^2 \\ PF7 &: \ 5.50\times10^{-7}\,\Omega/turn^2 \end{aligned} \qquad (22)$$

The evolutions of the radial and vertical components of poloidal error fields are shown in Fig. 5-1 and Fig. 5-2. Fig.6 is the change of the flux and the one-turn voltage at the center of the breakdown region. One finds that at 1.9 sec the poloidal error fields at the computation positions are less than 2mT and the one-turn voltage at the center is about 17V. Fig.s 7 are evolutions of coils currents. In Fig. 8, the optimized wave forms of control voltages of PF3, 4, 5, 6 and 8 are given. Fig. 9 is the time evolution of the total active power of converters. Fig. 10-1 and Fig. 10-2 are the configuration of the poloidal error field at time 1.8 sec and 1.9 sec in Fig. 5. At 1.9 sec, the region of error field less than 2mT appears at the breakdown region, which is as large as a disk of 1m radius.

As mentioned in section 1, the one-turn voltage required for the plasma breakdown is reduced with the help of additional heating. It is interesting to ask how the region of small error fields depends on the one-turn voltage. Figs. 11-1 to 11-4 are the results of optimizing breakdown when one-turn voltage at the center is about 10V. In this case, the radial error fields are kept small rather easily and only minimizing vertical components of the error field is needed. As shown in Fig. 11-3, the minimization of vertical field is more successful than Fig. 5-2. The region of small error field (< 2mT) in Fig. 11-4 is larger than that in Figs. 10 and looks more like circle.

Contours of 2mT error fields for one-turn voltage 17V, 14V and 10V are shown in Fig. 12. It implies that smaller one-turn voltage has an advantage of making region of small error field. For the breakdown of one-turn voltage less than 10V, the area of error field less than 2mT is slightly larger than that of 10V. Let us compare Fig. 12 with Fig. 4. One finds that the region of 2mT with one-turn voltage 10V is as large as that in Fig.4. Thus, this result implies that, reducing one-turn voltage as low as 10V, the error field pattern of initial magnetization is almost recovered by optimizing voltage wave form of PF coils.

In Fig. 13, it is shown the duration in which the error fields in the 1m circle at the breakdown region is less than 2mT as function of one-turn voltage at the center. One sees a remarkable increase of the duration as one-turn voltage is reduced. Since keeping region of small error field for a longer time gives more chance of the plasma initiation, low one-turn voltage at the center of breakdown region has a further advantage to obtain robust plasma breakdown.

5, Summary

BreakDown Optimization and Simulation (BDOS) code is developed, where the temporal wave forms of PF control voltages are optimized within given limitations. In the example of reference design of ITER EDA interim design, we have shown that optimization of PF voltages' wave form is possible so that the error field in a circle of 1m radius at the breakdown region is less than 2mT. Quantitative discussion is given on how lower one-turn voltage at the breakdown region provides advantages to initiating plasma discharge.

There are several ways to extend the survey on plasma breakdown. In this report, our analysis is performed using a simplified model of in-vessel components. Therefore, it is important to carry out the similar analysis using a detailed model which is conscientious to the present design of ITER EDA. It is interesting to investigate various breakdown scenarios, in which the positions and the pattern of flux supply are modified. It may be possible that there are optimum positions of plasma breakdowns, which are characteristic to each machine.

Although BDOS code deals only with initial plasma break down, the problem should be set to investigating the optimization of whole discharge, namely starting from plasma breakdown, current lamp up, heating, burning and plasma termination. There are several codes which have ability to simulate plasma discharge from lamp up to lamp down. We plan to use results of BDOS code as an initial configuration to such simulation codes. In this way, the optimization of the plasma discharge will be possible.

Acknowledgment

The authors are grateful to Dr. M. Matsukawa for useful discussions.

5, Summary

BreakDown Optimization and Simulation (BDOS) code is developed, where the temporal wave forms of PF control voltages are optimized within given limitations. In the example of reference design of ITER EDA interim design, we have shown that optimization of PF voltages' wave form is possible so that the error field in a circle of 1m radius at the breakdown region is less than 2mT. Quantitative discussion is given on how lower one-turn voltage at the breakdown region provides advantages to initiating plasma discharge.

There are several ways to extend the survey on plasma breakdown. In this report, our analysis is performed using a simplified model of in-vessel components. Therefore, it is important to carry out the similar analysis using a detailed model which is conscientious to the present design of ITER EDA. It is interesting to investigate various breakdown scenarios, in which the positions and the pattern of flux supply are modified. It may be possible that there are optimum positions of plasma breakdowns, which are characteristic to each machine.

Although BDOS code deals only with initial plasma break down, the problem should be set to investigating the optimization of whole discharge, namely starting from plasma breakdown, current lamp up, heating, burning and plasma termination. There are several codes which have ability to simulate plasma discharge from lamp up to lamp down. We plan to use results of BDOS code as an initial configuration to such simulation codes. In this way, the optimization of the plasma discharge will be possible.

Acknowledgment

The authors are grateful to Dr. M. Matsukawa for useful discussions.

Reference

[1] ITER EDA Design Description Document, Chapter 4.7, Poloidal field control.

[2] A. Kellman, Operation scenarios for ITER, ITER technical meeting on plasma equilibrium and control, April 1993. San Diego.

[3] ITER EDA Design Description Document, Chapter 1.9, Plasma physics.

[4] K. Nakamura and T. Koseki, JAERI-M 9612.
A. Kameari and Y. Suzuki, JAERI-M 7120.
A. Kameari, J. Comput. Phys., 42 (1981) 124.
S. Nishio, T. Horie, IEEE Transaction on Magnetics, 26 (1990) 865.

[5] T. Yamamoto, at Technical meeting of RF heating and current drive for ITER, 1993, Garching.
Private communication through T. Yamamoto et. al..

[6] For example INIMAG-code, private communication through T. Nishino, M. Hasegawa and K. Yoshida.

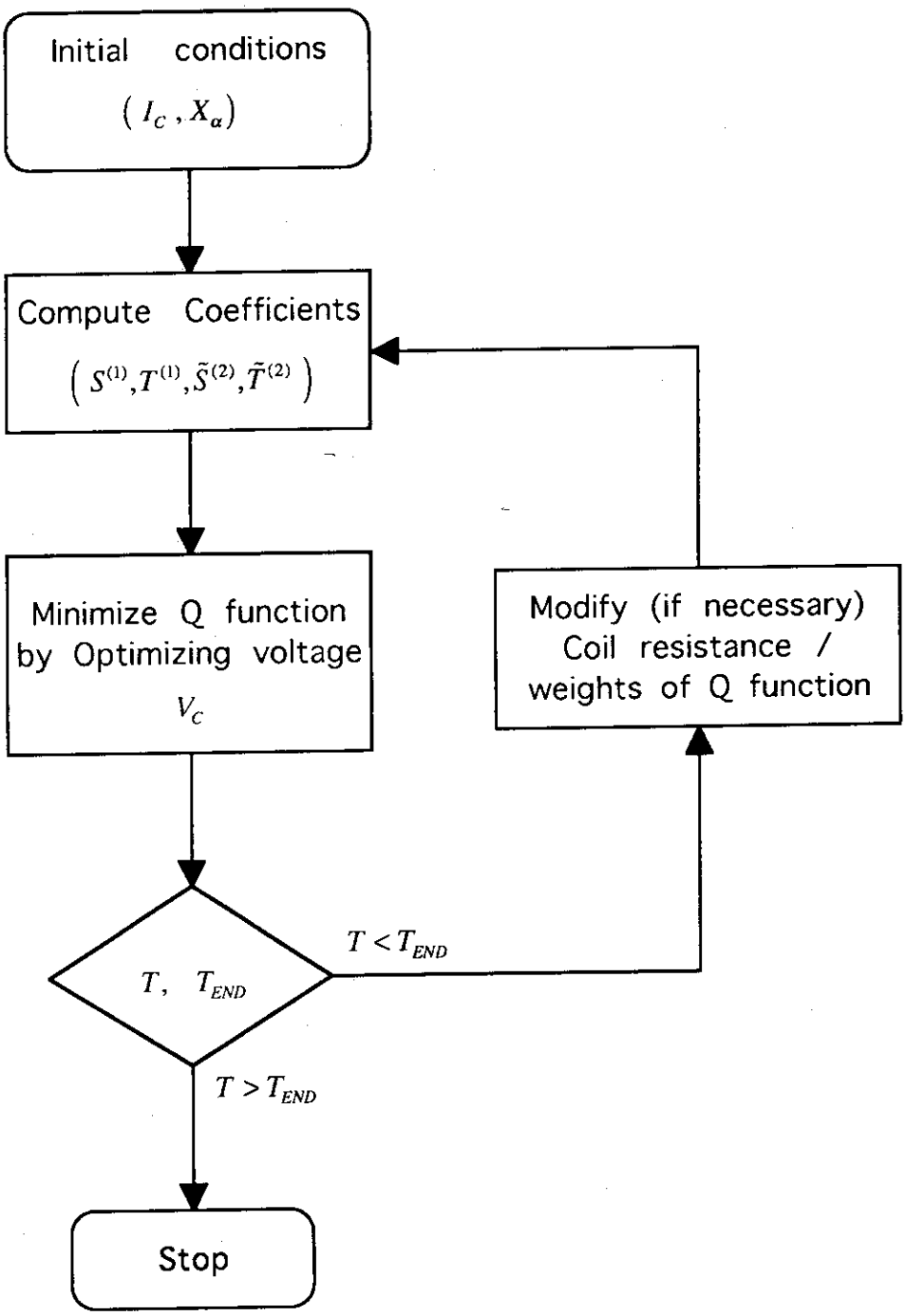

Fig. 1, Flow chart of BDOS code

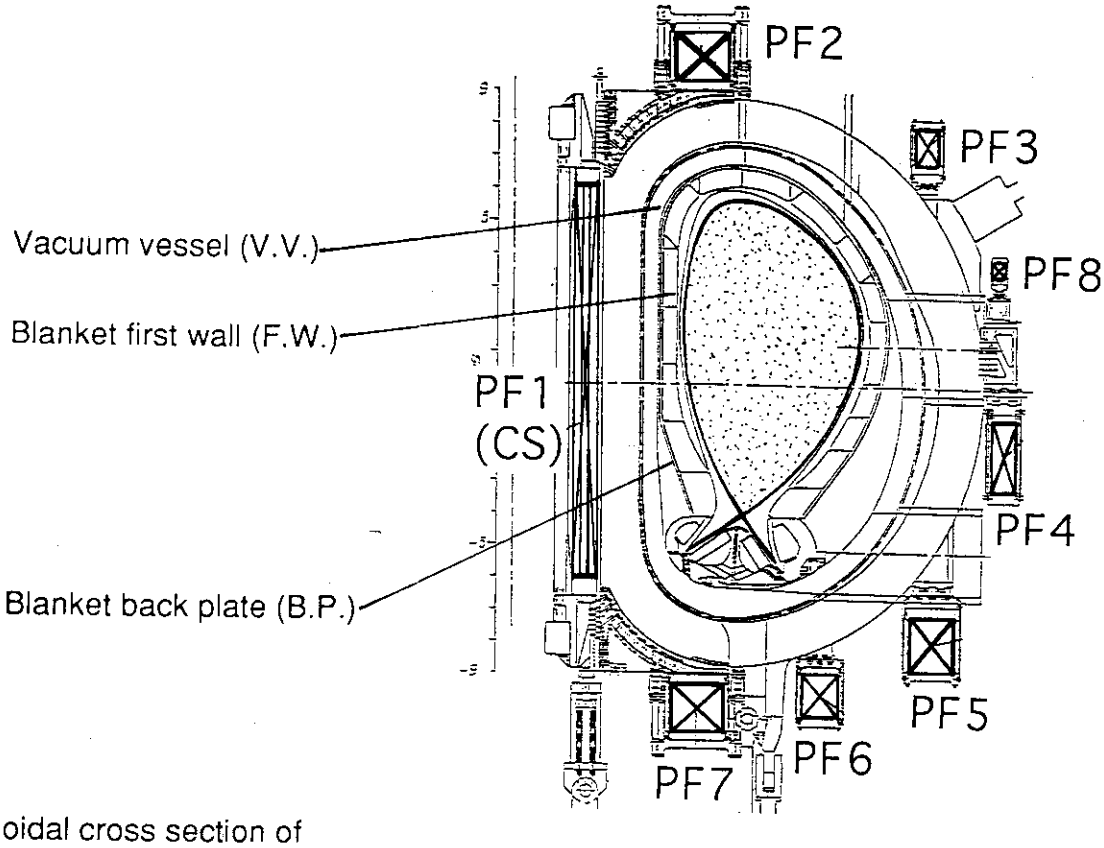

Fig. 2, Poloidal cross section of reference design of ITER EDA

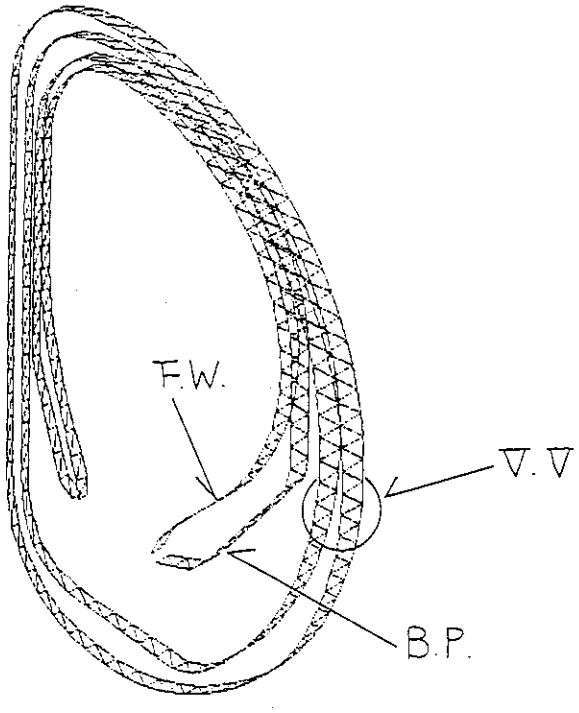

Fig. 3, Shell model of the reference design of ITER EDA

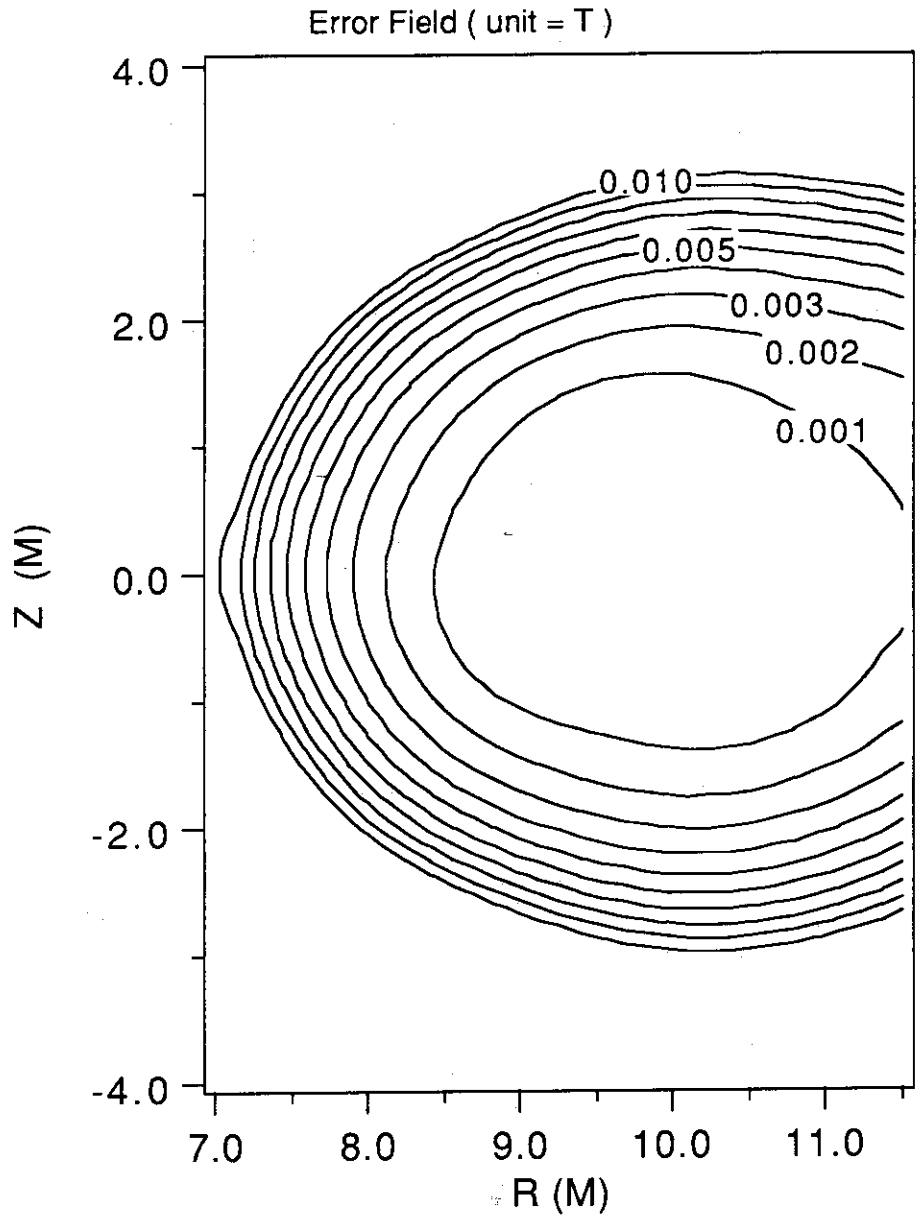

Fig. 4, The configuration of error field at the initial magnetization

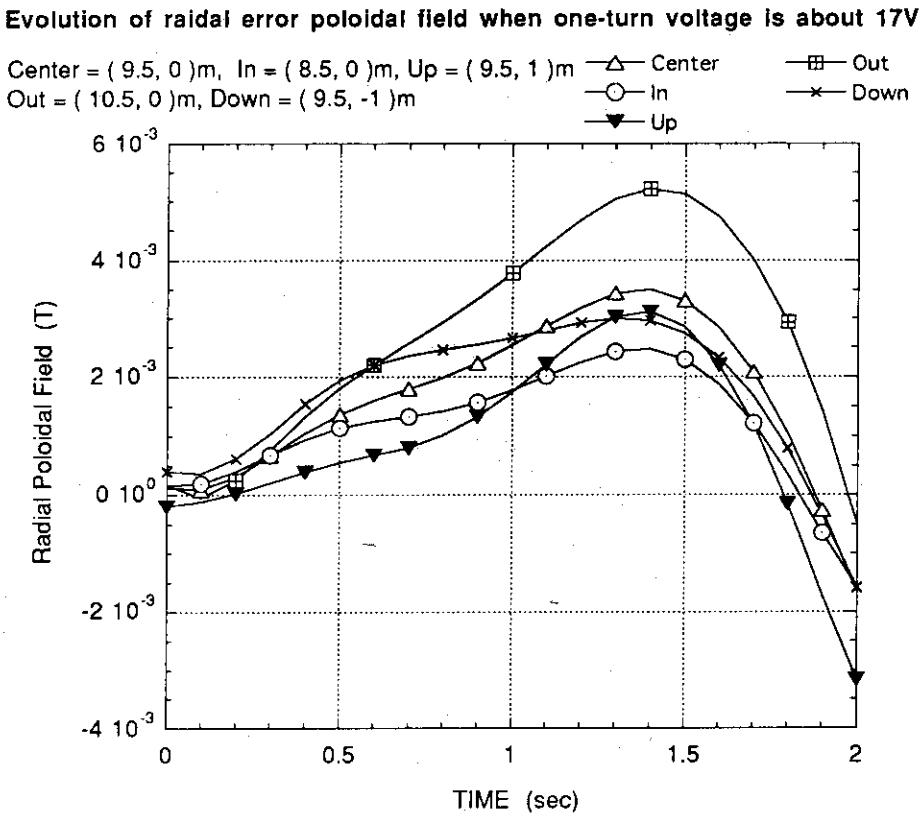

Fig. 5-1, The evolution of radial poloidal error field with 17V one-turn voltage

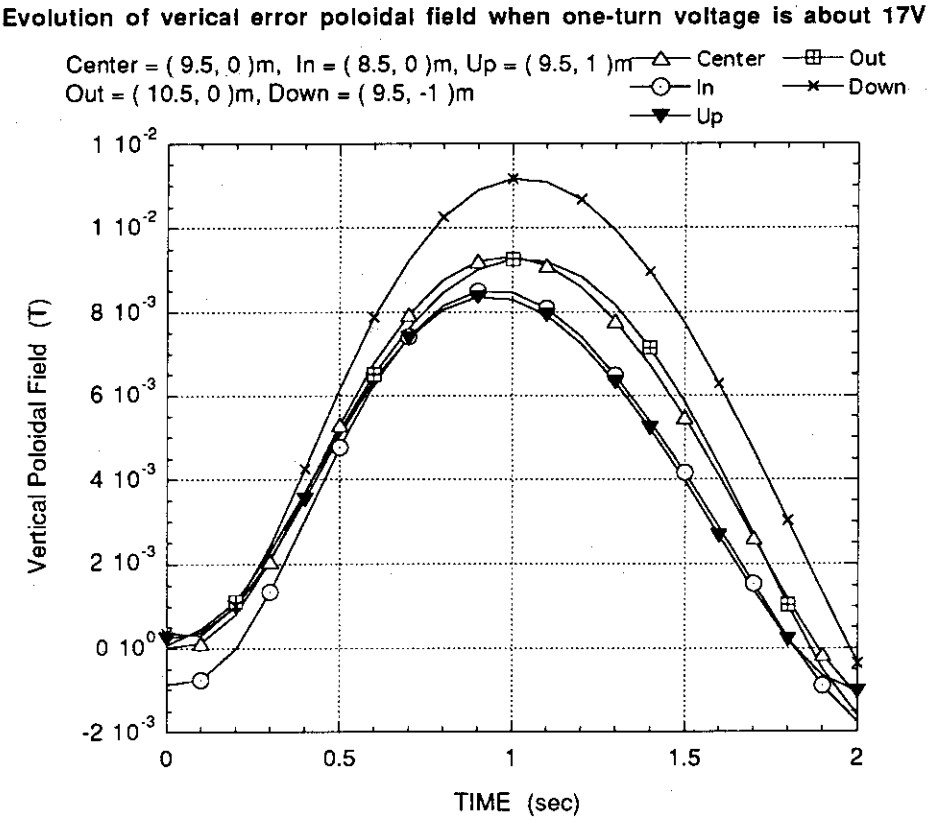

Fig. 5-2, The evolution of vertical poloidal error field with 17V one-turn voltage

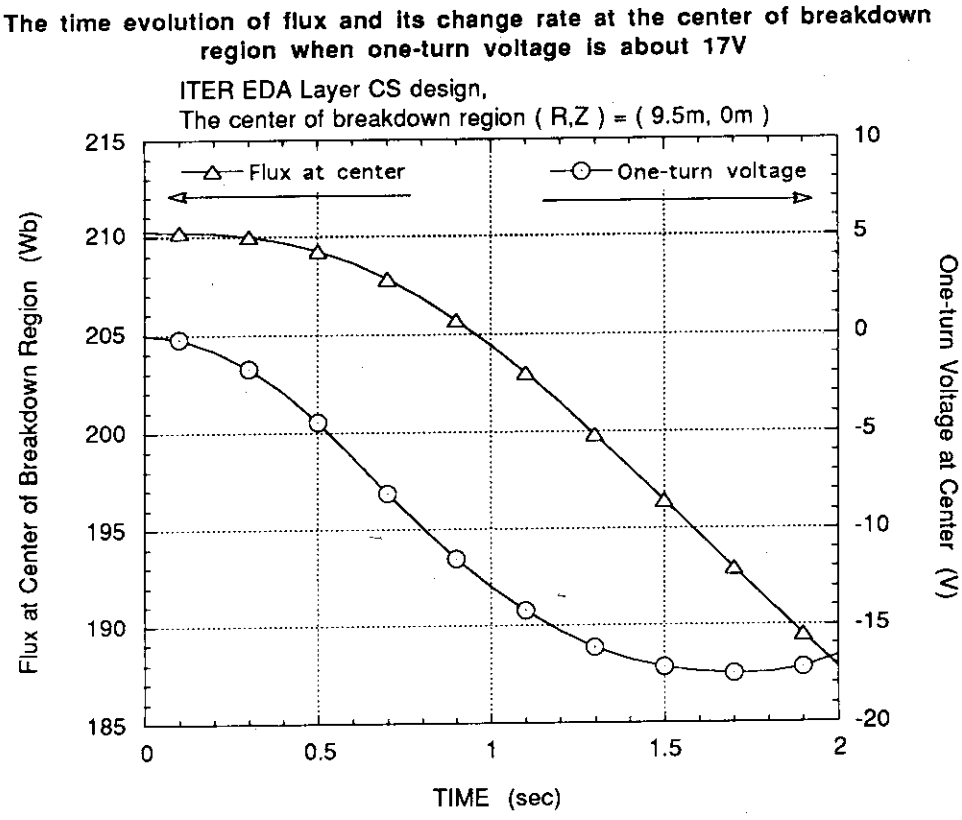

Fig. 6, The evolution of the flux at the center of breakdown region

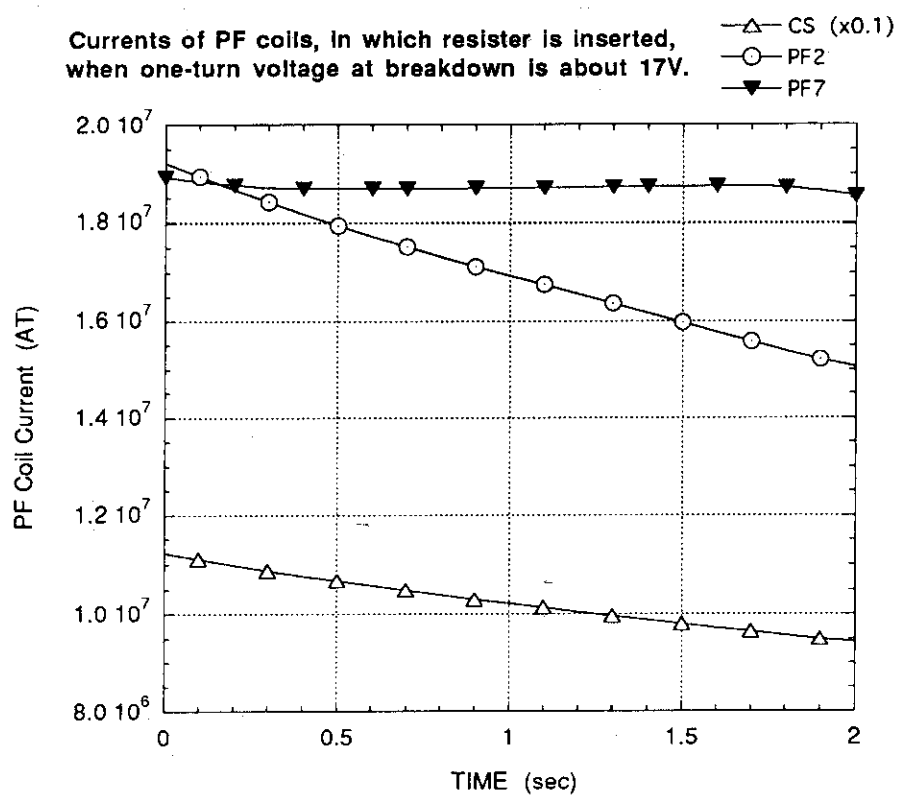

Fig. 7-1, The evolution of currents in CS, PF2 and PF7

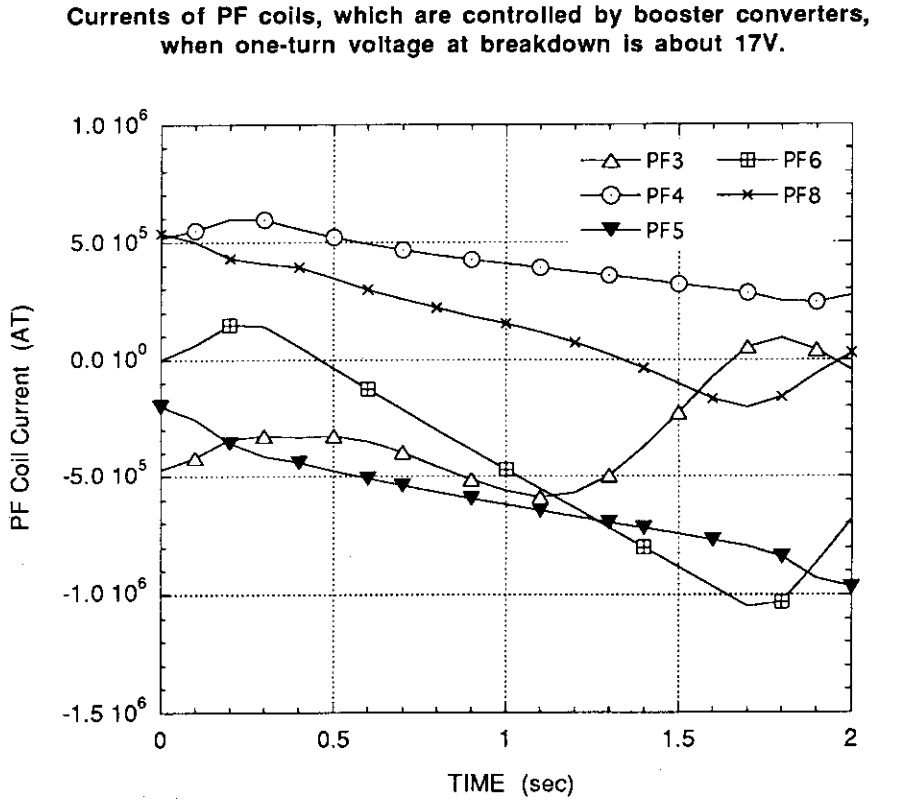

Fig. 7-2, The evolution of current in PF3, PF4, PF5, PF6 and PF8

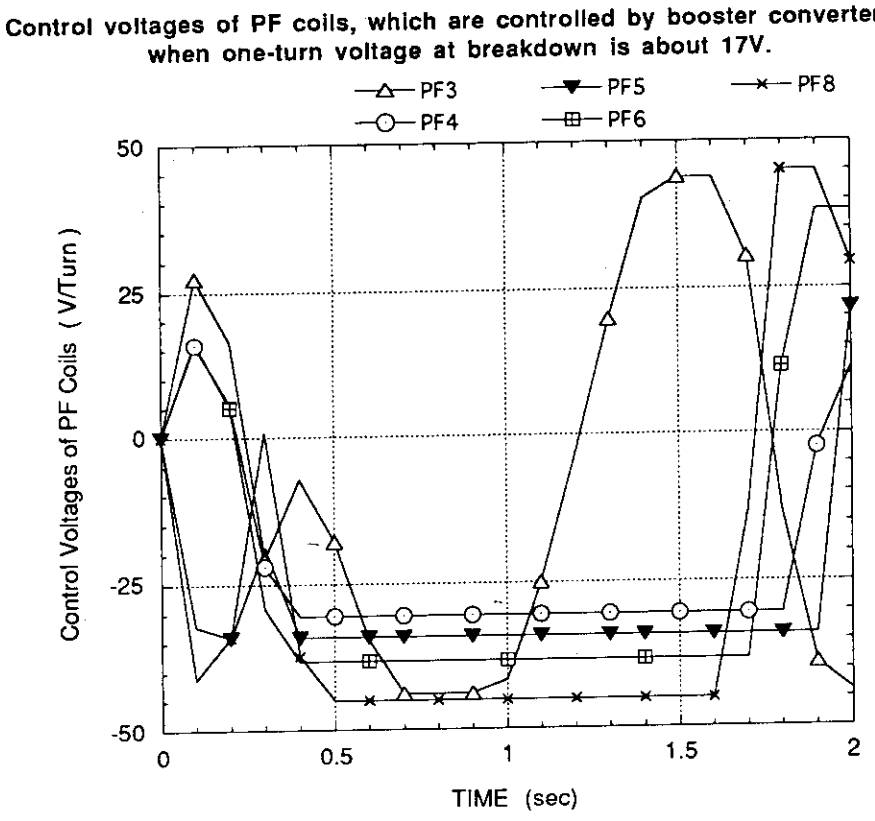

Fig. 8, Voltages of booster converters of PF3, PF4, PF5, PF6 and PF8

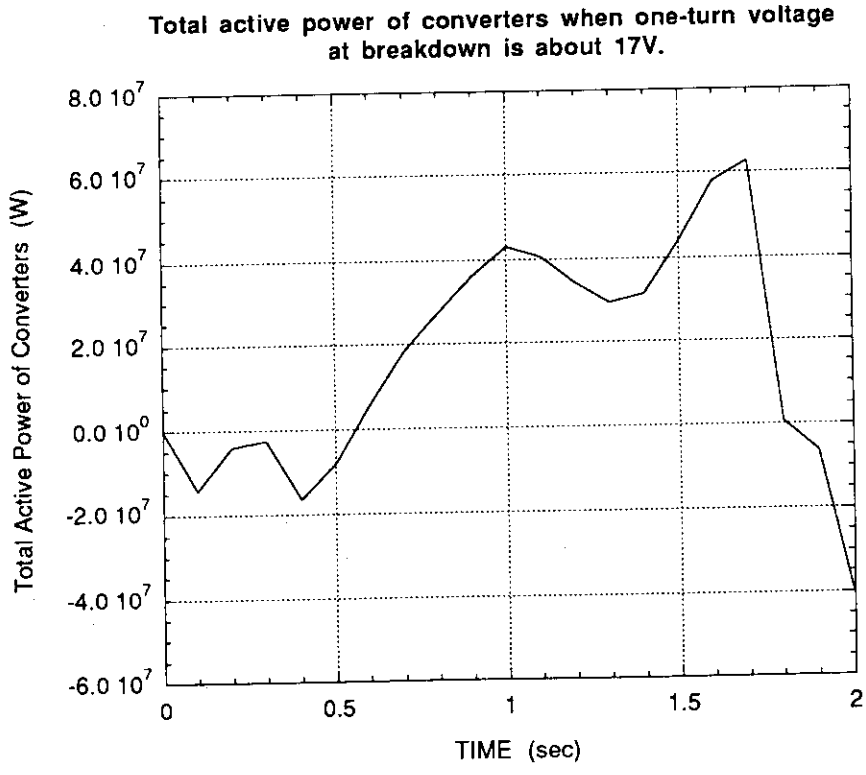

Fig. 9, Total active power of converters when one-turn voltage is 17V

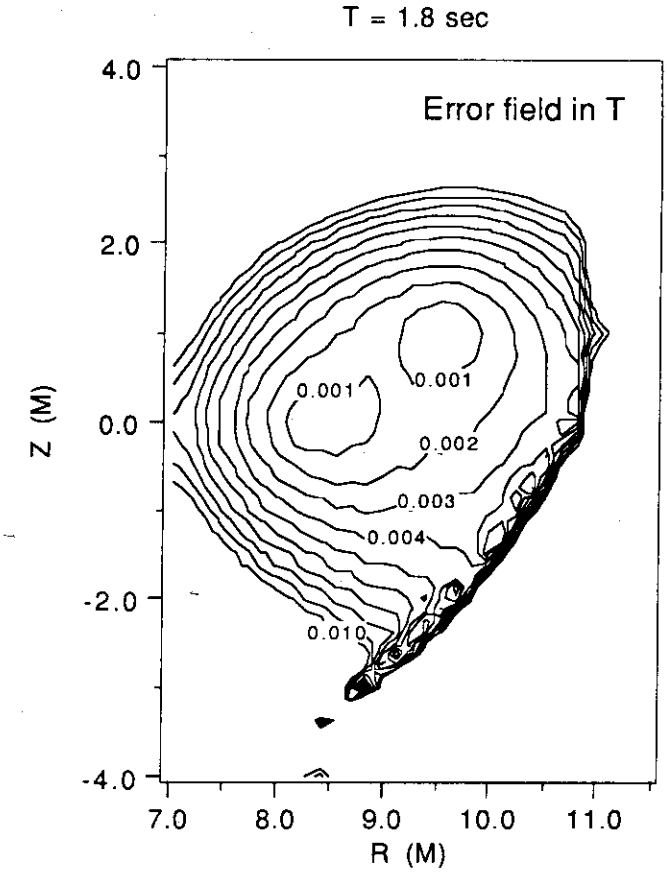

Fig. 10-1, Configuration of error field at T = 1.8 sec in Fig. 5.

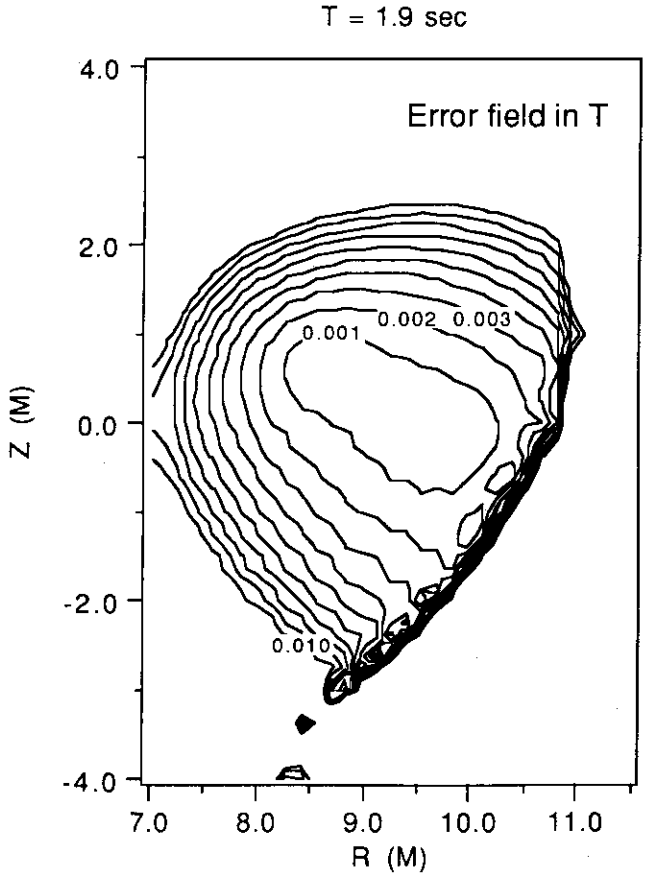

Fig. 10-2, Configuration of error field at T = 1.9 sec in Fig. 5.

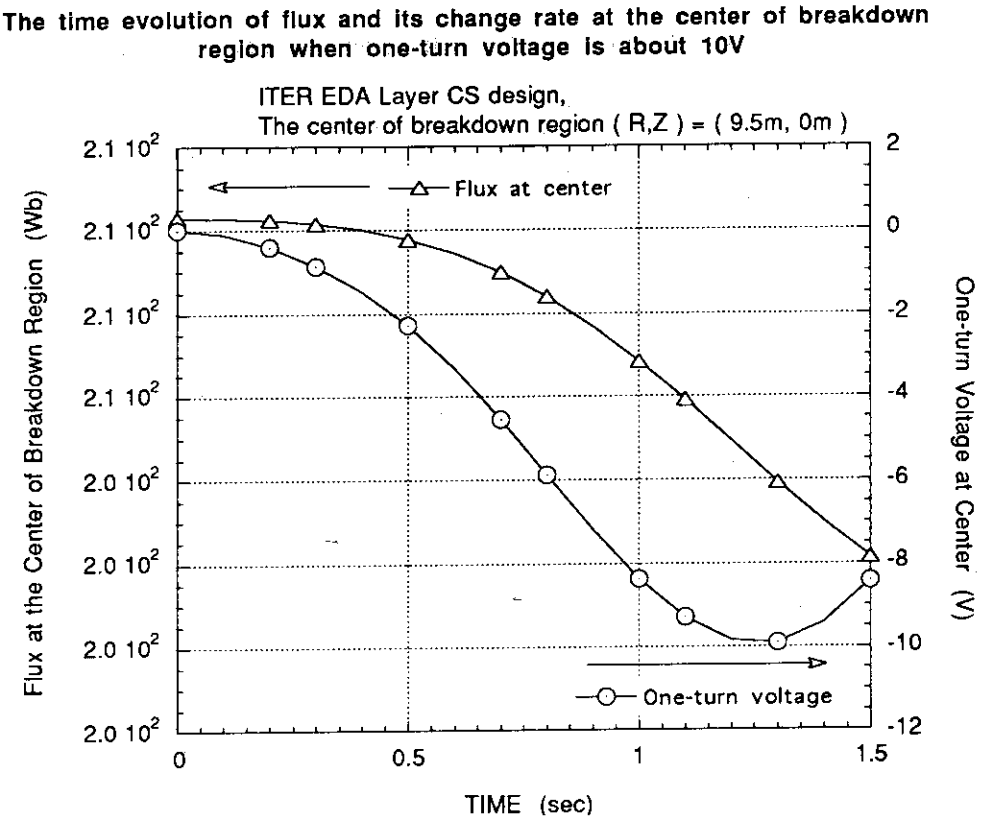

Fig. 11-1, The evolution of the flux when one-turn voltage is about 10V

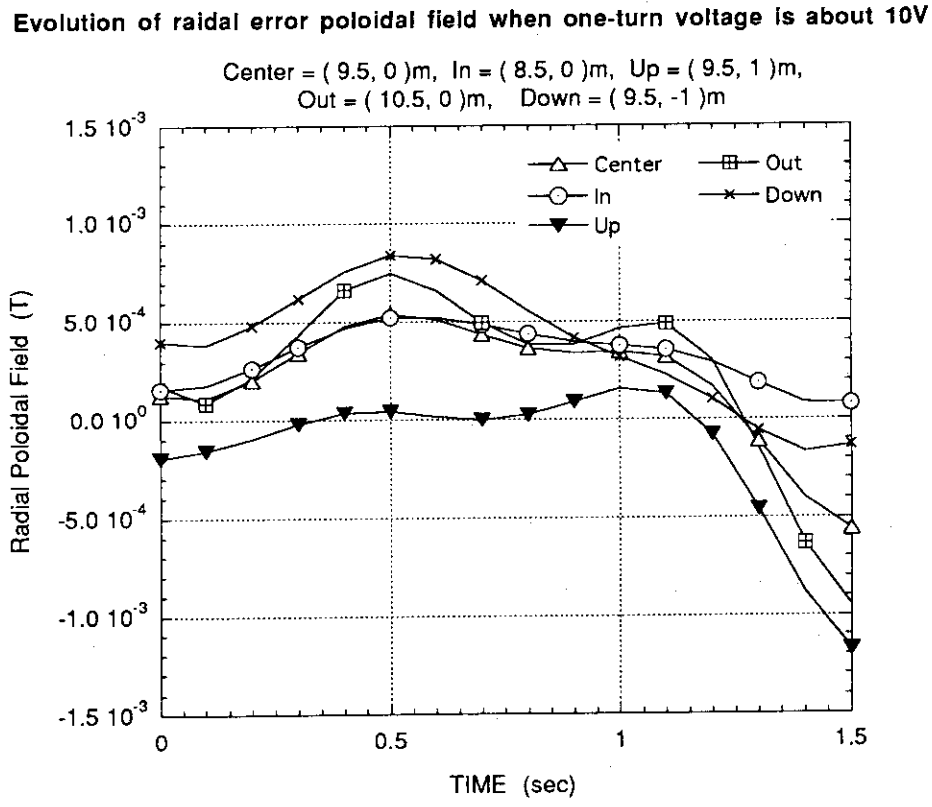

Fig. 11-2, The evolution of radial error field when one-turn voltage is about 10V

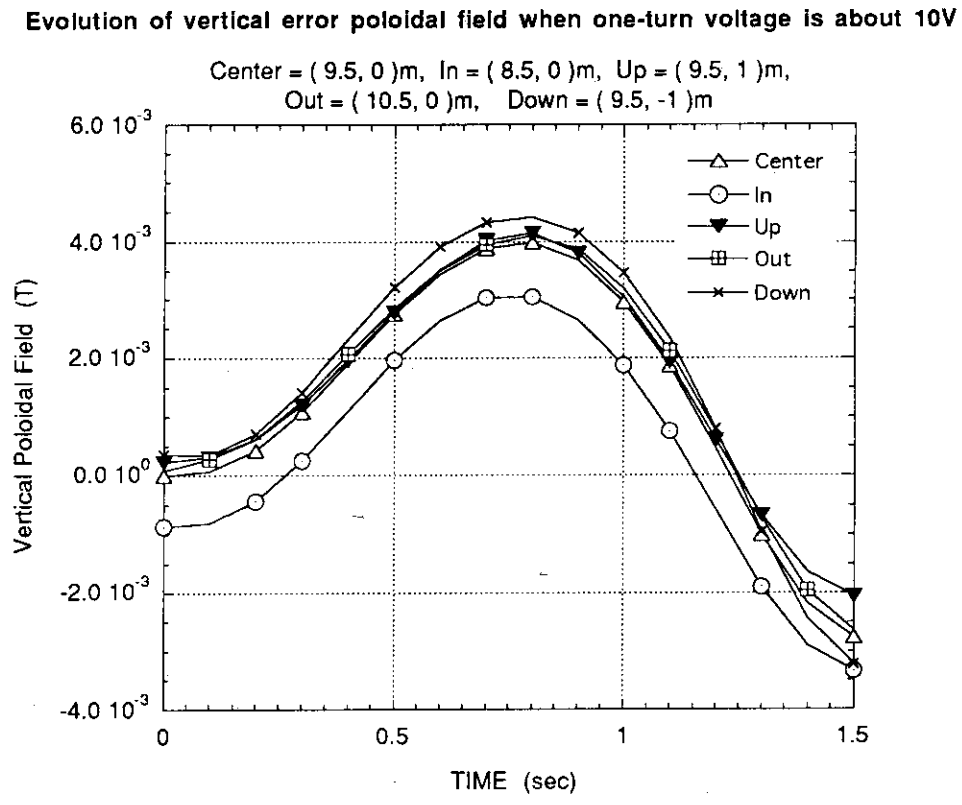

Fig. 11-3, The evolution of vertical error field when one-turn voltage is about 10V

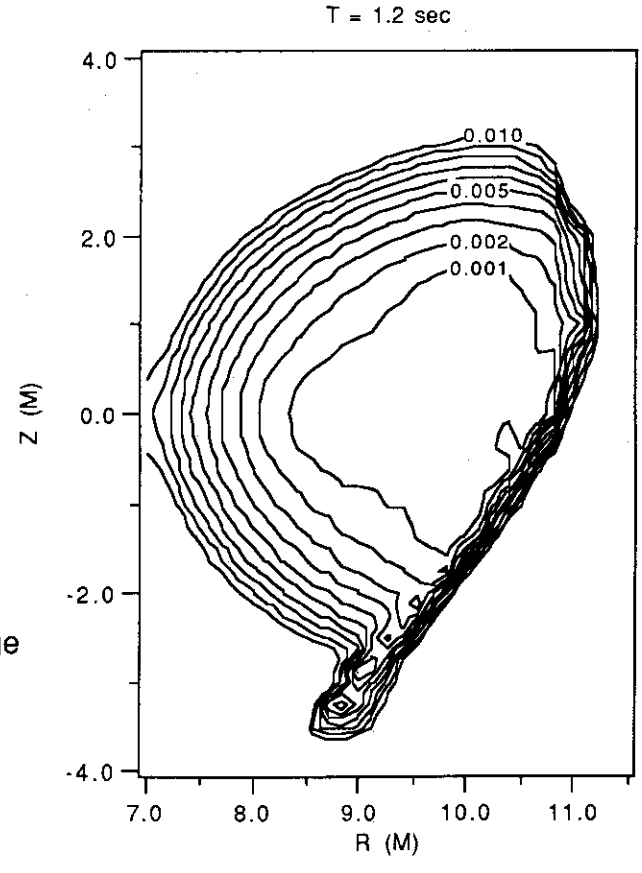

Fig. 11-4, The poloidal error field at T=1.2 sec when one-turn voltage at center is about 10V

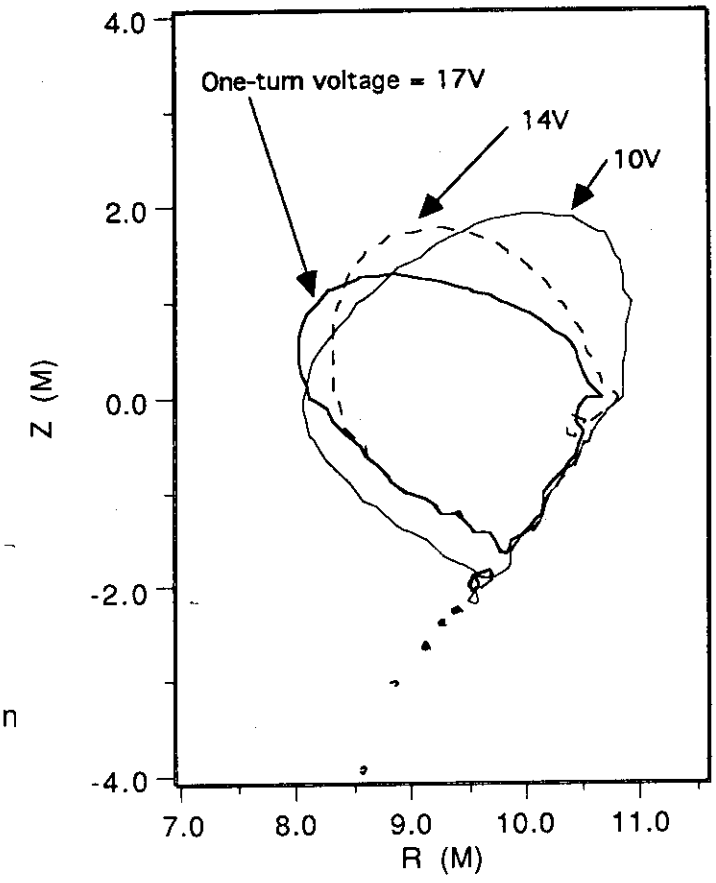

Fig. 12, Contours of 2mT for different one-turn voltage at the center of breakdown region

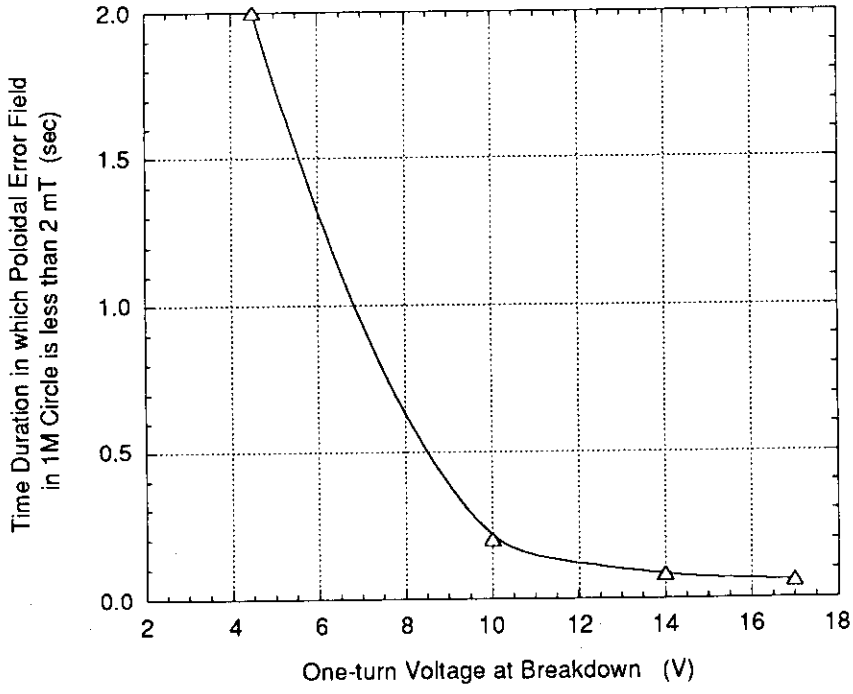

Fig. 13, The time duration in which poloidal error field in 1m circle at the breakdown region becomes less than 2mT vs. one-turn voltage